Transactions on Electrical and Electronic Materials (2019) 20:85–91
https://doi.org/10.1007/s42341-019-00104-y

Online ISSN 2092-7592
Print ISSN 1229-7607

REGULAR PAPER

Effect of Hydrogen Gas Conditions on the Structural, Optical, and Electronic Features of nc-Si:H Thin Films

Jae-Hyun Shim[1] · Ju-Han Kim[2] · Nam-Hee Cho[2]

Received: 18 December 2018 / Revised: 21 February 2019 / Accepted: 22 February 2019 / Published online: 16 March 2019
© The Korean Institute of Electrical and Electronic Material Engineers 2019

Abstract

Hydrogenated nanocrystalline Si (nc-Si: H) films were prepared by plasma enhanced chemical vapor deposition using SiH_4/H_2 gas. The Si nanocrystallites of the films consisted of Si–H_n (n = 1, 2, 3) bonds. The relative fraction of the Si–H bonds affected the size and volume fraction of the crystallites. Hydrogen radicals are essential for the formation of Si nanocrystallites. The Si nanocrystallite size increased from ~ 2.0 to ~ 3.0 nm with an increase in the H_2 flow rate from 60 to 90 sccm. At the H_2 flow rate of 90 sccm, the film became completely polymeric consisting mainly of Si–H-type bonds.

Keywords Silicon · Plasma enhanced chemical vapor deposition · Photoluminescence · Nanostructure · Nanocrystallite · Chemical bonding

1 Introduction

Over the past few years, various studies have been carried out to investigate the structure and properties of hydrogenated nanocrystalline silicon (nc-Si:H) thin films containing Si nanocrystallites (< 5 nm) in a hydrogenated amorphous silicon (a-Si:H) matrix [1] because of their improved electronic and optical properties compared to those of their amorphous counterparts for device applications [2, 3]. The physical properties of nc-Si:H films can be ascribed to the quantum confinement effect (QCE), which is induced by the presence of Si nanocrystals of the size of several nanometers in them ($E_g = 1.7$ eV). The quantum confinement effect enables nc-Si:H films to absorb light in a wider visible region [4]. Plasma enhanced chemical vapor deposition (PECVD) is widely used to manufacture nc-Si:H films for applications in electronic and optoelectronic devices [5]. The size of these films and their Si nanocrystalline fraction affect their electronic and optical properties. The nanocrystallite formation mechanism, which determines the film structure, is controlled by the interactions between the hydrogen atoms of the plasma and the solid silicon matrix [6].

Source gas introduction conditions play an important role in the growth of nc-Si:H films by the PECVD method. This is because these conditions can affect many processes during the film growth such as selective etching, chemical etching, and thermal kinetic processes. Among the deposition conditions, hydrogen components are especially important for controlling the size and volume fraction of the Si nanocrystals in the films. In the PECVD method, silane (SiH_4) diluted with hydrogen gas is used as the precursor for nc-Si:H films. When nanocrystalline Si is formed in the films, hydrogen mixes with amorphous silicon (a-Si) and the dangling bonds in the microvoids or multivacancies saturate with hydrogen atoms to promote crystallization [7]. Hydrogen radicals remove the hydrogen bonds from the surface, generating nucleation and growth sites for Si nanocrystallites [8, 9]. The formation of hydrogenated amorphous or micro/nanocrystalline Si (a-Si:H and mc/nc-Si:H) is controlled by the precursor gases and substrates.

In this study, the effect of the H_2 flow rate (at a constant SiH_4 flow rate) on the nanostructural and chemical bonding characteristics of nc-Si:H films was investigated In particular, the chemical bonds between Si and hydrogen were analyzed by Fourier transform infrared (FT-IR) spectroscopy and X-ray photoelectron spectroscopy (XPS) to investigate the effects of the chemical features of the amorphous matrix on the nanostructural evolution of the films. We also

✉ Nam-Hee Cho
jhshim@dsu.ac.kr

1 Department of Advanced Materials and Energy Engineering, Dongshin University, Naju 58245, Republic of Korea

2 Department of Materials Science and Engineering, Inha University, Incheon 402-751, Republic of Korea

investigated the relationship between the nanostructural evolution of the films and their chemical, optical, and electrical characteristics.

2 Experimental

Nc-Si:H thin films were deposited on p-type Si (001) wafers with a specific resistance of 1–30 Ω cm using the PECVD method. SiH_4/H_2 gas was used as the precursor, and an radio frequency (RF) power of 100 W was used. H_2 was introduced into the evacuated chamber at the flow rates of 45, 60, 75, and 90 sccm, while the SiH_4 flux was maintained at 10 sccm. The base pressure of the chamber was 1.33×10^{-3} Pa. The films were deposited at room temperature for 3 h. Al:ZnO thin films with a thickness of 100 nm were deposited on the surface of the nc-Si:H films by RF magnetron sputtering and were used as transparent conducting electrodes for *I–V* measurements.

The nanostructure of the nc-Si:H thin films was examined by transmission electron microscopy (TEM, Philips EM430). The size and volume fraction of the Si crystallites in the films were measured from the intensity distribution of their Raman spectra. The Raman measurements were carried out on a T64000, Jobin–Yvon analysis system using a 514 nm Ar laser. FT-IR absorption measurements were carried out at 1900–2400 cm^{-1} on a Bruker-IFS66v/s spectrometer. XPS analysis was carried out on a PHI 5700 electron spectroscope (ESCA) using monochromatic Mg-Kα radiation. The binding energy calibration was carried out by using the energy position of the C1 s core level of contamination carbon. The pressure in the analysis chamber was maintained at $< 2 \times 10^{-7}$ Pa. The accuracy of the binding energy values was 0.1 eV. X-ray diffraction (XRD) measurements were carried out at room temperature on an X' Pert PRO MRD-Phillips instrument operating in the standard θ–2θ configuration with Cu-Kα radiation (1.5406 Å). The photoluminescence (PL) properties of the samples at 300 K were analyzed using a spectrofluorophotometer (SPEX, 1403) with a He–Cd laser (325 nm) as the excitation source. The *I–V* characteristics of the samples were measured using a Keithley 236 electrometer in the dark.

3 Results and Discussion

3.1 Structural Features

Figure 1a shows the XRD patterns of the nc-Si:H films. The diffraction peaks at $2\theta = 28.4$ and 47.3° correspond to the (111) and (220) planes of Si, respectively. The (111) Si diffraction peak for the films prepared with the H_2 flow rate of 60 sccm (2) was broad (full width at half-maximum, FWHM: ~ 4.71°), while the films prepared with the H_2 flow rates of 75 (3) and 90 sccm (4) showed relatively sharp diffraction peaks (FWHM: ~ 2.41 and ~ 2.06°, respectively). The film prepared at the H_2 flow rate of 45 sccm (1) did not exhibit any noticeable crystalline Si peaks. It is believed that nc-Si:H films prepared in the presence of H_2 flow show nearly pure amorphous Si structure.

The average nanocrystallite size of the films was also determined from the FWHM of their (111) XRD diffraction peaks using the Scherrer's equation, [10] which corresponds to the broad fits in Fig. 1.

$$d = \frac{K\lambda}{\beta \cos \theta} \tag{1}$$

In Eq. 1, d is the average crystallite size, β is the FWHM of the diffraction peak, θ is the Bragg angle, λ is the X-ray wavelength, and $K = 0.94$ is the Scherrer constant.

The average Si nanocrystallite sizes of the films prepared at the H_2 flow rates of 60, 75, and 90 sccm were found to be ~ 1.9, ~ 3.0, and ~ 4.3 nm, respectively. These values were obtained from the best fits, and some of the relevant fits are shown in Figs. 1b–d.

Figure 2 shows the Raman spectra of the nc-Si:H films prepared at the H_2 flow rates of (a) 45, (b) 60, (c) 75, and (d) 90 sccm. A sharp peak was observed at 521 cm^{-1} in Fig. 2d. A noticeable variation in the spectra of the films prepared at different H_2 flow rates was observed over the frequency range of 500–520 cm^{-1}. The Raman spectra of the films were deconvoluted, and the best fits are shown in each spectrum in Fig. 2. The fits were observed at 480, 390, and 310 cm^{-1} corresponding to the transverse optics (TO), longitudinal optics (LO), and longitudinal acoustics (LA) modes of a-Si, respectively. On the other hand, the films prepared at the H_2 flow rates of 60, 75, and 90 sccm showed small peaks at 508.7, 510.9, and 512.4 cm^{-1}, respectively corresponding to nc-Si:H.

The Raman spectrum of bulk Si shows a single sharp transverse optical mode at 520 cm^{-1}; the other Raman modes are not active. However, in the case of small Si crystals with the size of a few nanometers, the momentum conservation during the transfer process relaxes and the Raman activation mode is not limited to the center of the Brillouin zone. Consequently, the presence of such Si nanocrystallites produces a small peak in the Raman spectrum over the frequency range of 520 to ~490 cm^{-1} depending on the crystallite size [11–13].

The Raman line shape of Si nanocrystallites can be determined by the phonon confinement effect [14]. The following formula (Eq. 2) was used to estimate the mean crystallite size (d):

$$d = 2\pi \sqrt{\frac{B}{\Delta\omega}} \tag{2}$$

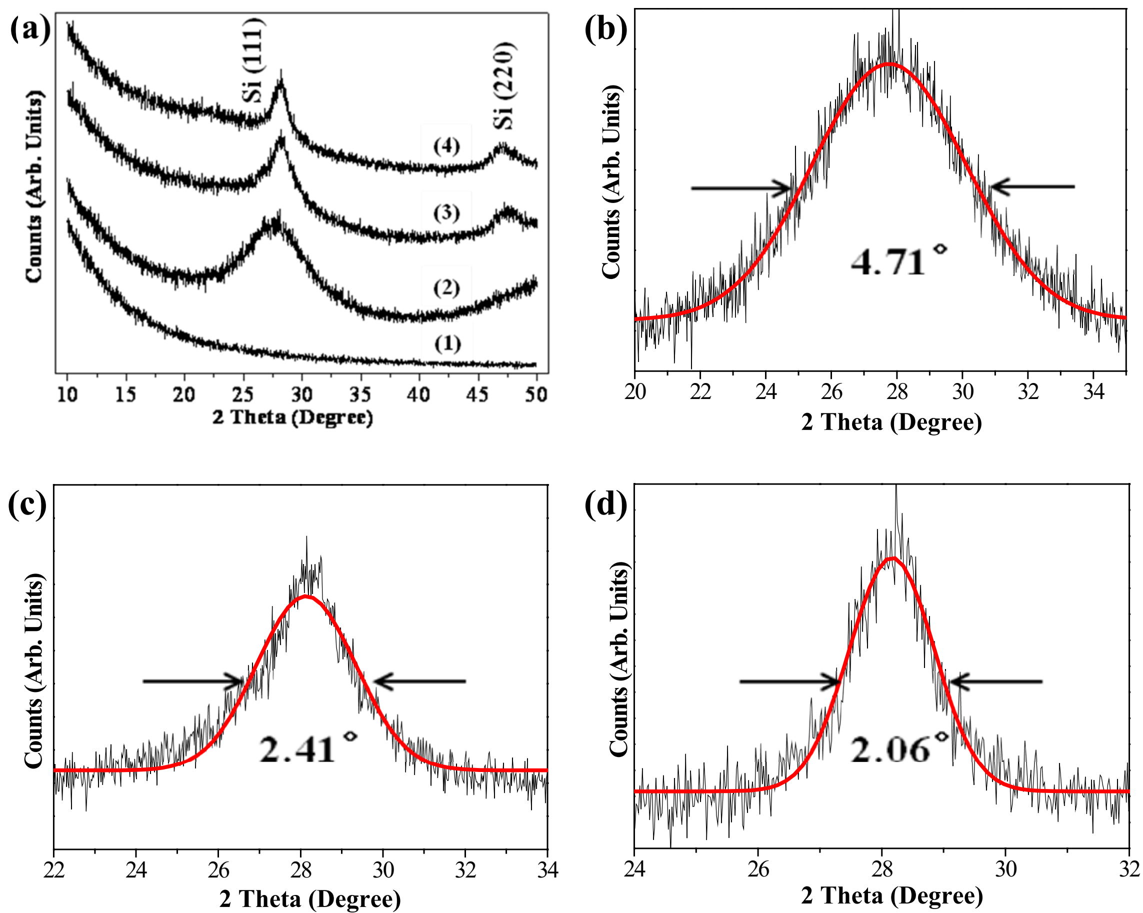

Fig. 1 **a** XRD patterns of the films prepared at the H_2 flow rates of 45 (1), 60 (2), 75 (3), and 90 (4) sccm. Enlarged (111) XRD peaks of the films prepared at the H_2 flow rates of **b** 60, **c** 75, and **d** 90 sccm

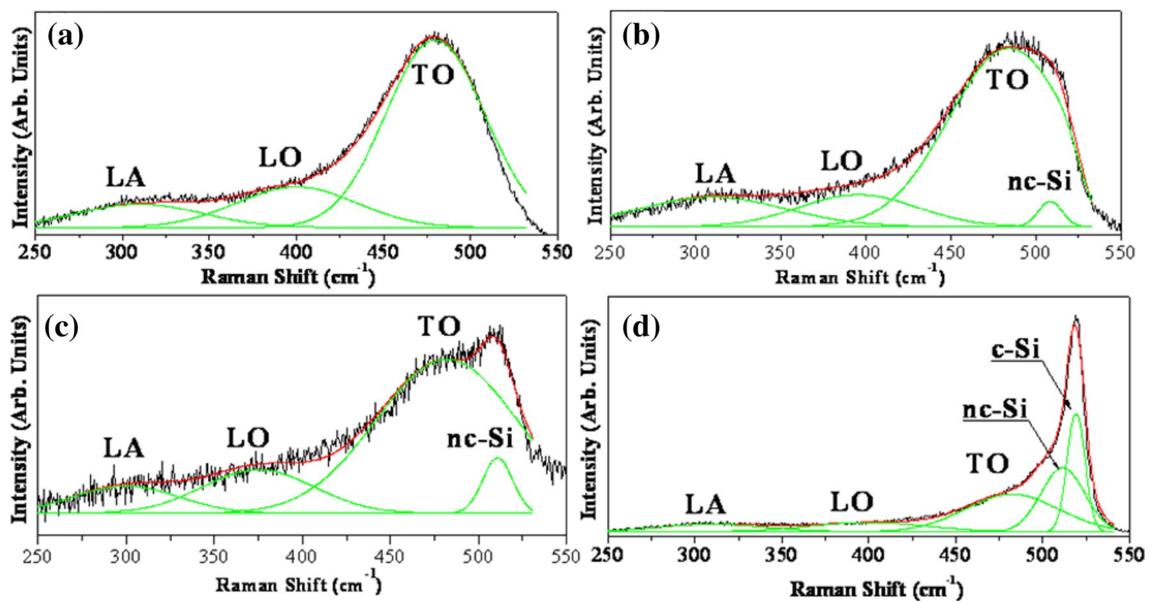

Fig. 2 Raman spectra of the nc-Si:H films deposited at the H_2 flow rates of **a** 45, **b** 60, **c** 75, and **d** 90 sccm. The spectra were deconvoluted and their best fits are illustrated

where Δω is the shift in the peak position of nc-Si compared to that of bulk Si and $B = 2.0$ cm^{-1} nm^2.

With an increase in the H_2 flow rate from 60 to 90 sccm, Δω decreased from 11.3 to 8 cm^{-1}, as shown in Fig. 2. This suggests that the crystallite size increased from ~ 2.3 to ~ 3.1 nm. However, no noticeable fit corresponding to nc-Si was observed in the Raman spectra of the film prepared at the H_2 flow rate of 45 sccm, indicating the absence of Si nanocrystallites in it.

Figure 3 shows high-resolution TEM (HRTEM) images of the films prepared at the H_2 gas flow rates of (a) 60 and (b) 90 sccm. These films consisted of Si crystals with a particle size of ~ 2–4 nm. It is likely that the micrographs showed only the nanocrystallites with a low index zone parallel to the incident electron beam. When the deposition was carried out at the SiH_4 gas flow rate of 60 sccm, lattice planes with a spacing of 3.1 Å could be observed, as shown in Fig. 3a. The observed interplanar distance corresponds to the {111} plane of crystalline Si. In the case of the nc-Si:H film prepared at the H_2 gas flow rate of 90 sccm, a large number of lattice planes with high density were observed. This film showed lattice spacings of 1.9 and 3.1 Å corresponding to the {220} and {111} planes (Fig. 3b). The main orientation [110] of the nanocrystalline Si was observed in the inset of Fig. 3b, which is the fast Fourier transformation of the micrograph. Some {220} and {111} diffraction spots for nanocrystalline Si can also be observed in the inset.

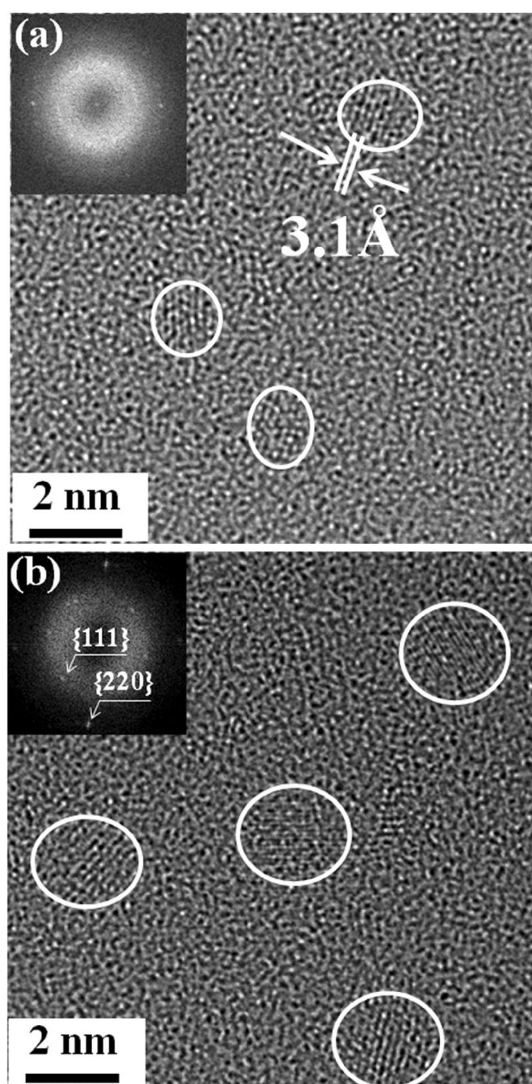

Fig. 3 HRTEM images of the nc-Si:H thin films prepared at the H_2 flow rates of **a** 60 and **b** 90 sccm. A few nanocrystallite regions are denoted with white circles

Table 1 lists the crystallite sizes of the films determined by the XRD, Raman spectroscopy, and TEM analyses. The XRD results were in good agreement with the Raman spectroscopy results. On the other hand, a considerable discrepancy was observed in the crystallite sizes of the film prepared at the H_2 flow rate of 90 sccm measured by the XRD (3.1) and Raman spectroscopy (4.3) analyses. This can be attributed to the difference in the crystallite size ranges of these measurement techniques, which can comprise the characteristic spectrum features. Another reason for this difference can be the physical characteristics of the crystallites such as the strain and chemical bonds. These characteristics can cause some additive effects on the size-dependent spectra features in the measurements.

The volume fraction (X_c) of nanocrystalline Si was obtained from two fits of the Raman spectra. One was the crystalline component, I_c, as obtained from the integrated Raman scattering intensity at 500 ± 15 cm^{-1}, while the other was the amorphous component I_a at ~ 480 cm^{-1}. The ratio of the volume fraction of the crystallites is defined as $X_c = I_c/(I_c + \eta I_a)$, where η is the scattering factor. For the crystallites with the size of a few nanometers, η is considered to be ~ 1.0 [15]. Nanocrystalline Si was formed at the H_2 flow rates of 60–90 sccm. The film obtained at the H_2 flow rate of 45 sccm was completely amorphous. The volume fraction of the crystallites increased from ~ 2.7 to ~ 34.2% with an increase in the H_2 flow rate from 60 to 90 sccm.

Table 1 Crystallite sizes of the nc-Si:H films prepared at various H_2 flow rates obtained from the XRD, Raman spectroscopy, TEM, and PL measurements (d_{XRD}, d_{Raman}, d_{TEM}, and d_{PL}, respectively). E is the energy bandgap obtained from the PL spectra

H_2 flow rate (scan)	$d_{XRD(mm)}$	$d_{Raman(mm)}$	$d_{TEM(mm)}$	$d_{PL(mm)}$	E (eV)
45	–	–	–	–	–
60	1.9	2.3	2.0	2.3	2.00
75	3.0	2.6	2.7	2.8	1.87
90	4.3	3.3	3.0	3.2	1.80

3.2 Chemical Features

Figure 4 shows the FT-IR spectra of the nc-Si:H films prepared at the H_2 flow rates of (a) 45, (b) 60, (c) 75, and (d) 90 sccm. The spectra were deconvoluted and the best fits were obtained. The prominent peak at 2000 cm^{-1} can be attributed to the stretching vibration of the Si–H bond (mono-hydride), while two peaks at 2100 and 2140 cm^{-1} correspond to the stretching vibrations of the Si–H_2 and Si–H_3 bonds, respectively [16].

The intensity of the peak at 2000 cm^{-1} increased with an increase in the H_2 flow rate (up to 90 sccm). This indicates that the dominant silicon-hydrogen bonds transformed from Si–H_2 to Si–H with an increase in the H_2 flow rate (up to 90 sccm).

The relative fractions of the Si–H bonds, $\frac{Si-H}{\sum_{n=1}^{3} Si-H_n}$, in the films prepared at the H_2 flow rates of 45, 60, 75, and 90 sccm were 0.066, 0.245, 0.635, and 0.702, respectively. The fraction of the Si–H bonds increased steadily with an increase in the H_2 flow rate.

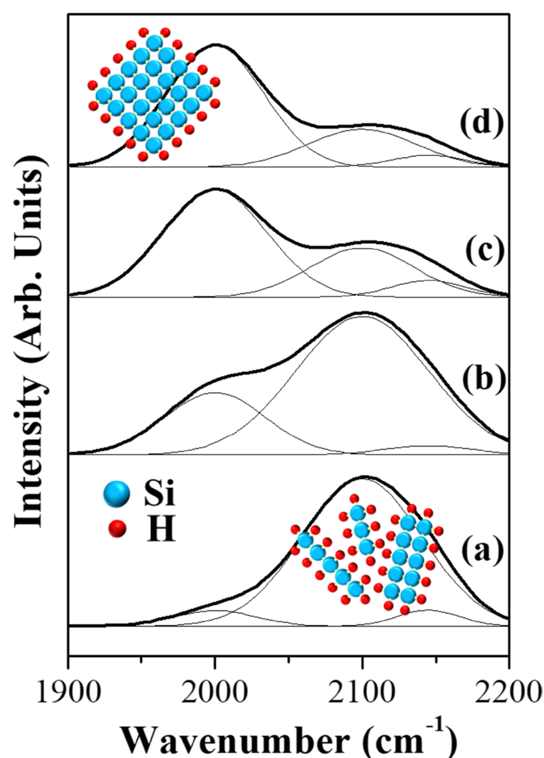

Fig. 4 FT-IR absorption spectra of the nc-Si:H films prepared at the H_2 flow rates of **a** 45, **b** 60, **c** 75, and **d** 90 sccm. The spectra were deconvoluted and their best fits are illustrated. Schematic of the nanocrystallites **a** and amorphous matrix **b** in the nc-Si:H films. The surface of the nanocrystallites was passivated mostly by Si–H bonds. The amorphous matrix contained silicon clusters consisting mainly of Si–H_3 and Si–H_2 bonds

Figure 5 shows the Si2p binding energy of the nc-Si:H films prepared at the H_2 flow rates of (a) 45, (b) 60, (c) 75, and (d) 90 sccm With an increase in the H_2 flow rate from 45 to 90 sccm, the binding energy of the Si2p electrons (from 99.1 to 99.6 eV) and the intensity of the Si2p peaks increased, while the intensity of the SiH_x 2p peak at 102.9 eV decreased without any shift in the binding energy. The Si2p peak shifted from 99.1 to 99.6 eV because of the modified Si–Si bonds [17]. This is because the breakage of Si–H bonds makes Si–Si bonds strong. This can be evaluated on the basis of the Si2p peak integration intensity, which is proportional to the S–Si bond content. With an increase in the H_2 flow rate, the Si2p integral intensity increased, indicating a decrease in the number of the Si–H bonds and an increase in the number of the Si–Si bonds.

The relative volume fraction of the Si crystallites increased with an increase in the H_2 flow rate. As shown in Fig. 4, most of the Si–H, Si–H_2, and Si–H_3 bonds were located on the surface of the Si nanocrystals or in the polymeric Si clusters in the nc-Si:H films. Since the crystallite size ranged from ~ 2.0 to ~ 4.0 nm, it can be stated that the surface of the crystallites was passivated mainly by the Si–H bonds, as shown in Fig. 4a. On the other hand, the presence of the Si–H_2 and Si–H_3 bonds can be attributed to the polymeric chains consisting of the Si–H_3 and Si–H_2 bonds in the matrix of the films (Fig. 4b) [18]. Hence, the change in the relative volume fraction of the Si crystallites can be attributed to the relative fraction of the Si–H bonds, $[Si-H] / \sum [Si-H_n]_{n=1,2,3}$, in the films. The Si–H bonds played a key role in passivating the surface of the crystallites. In addition, the relative fraction of the Si–H_3 and Si–H_2 bonds decreased with an increase in the relative volume fraction of the Si nanocrystallites embedded in the amorphous matrix, as shown in Fig. 4.

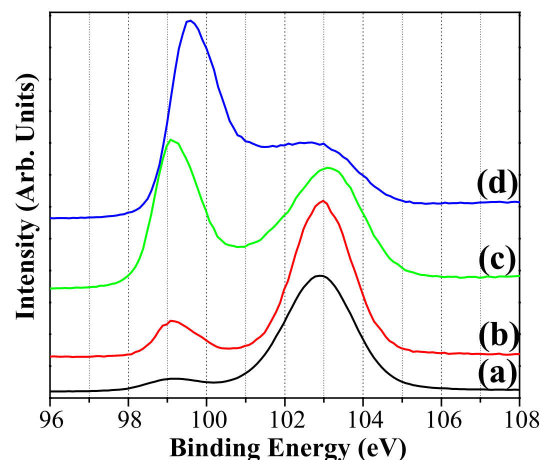

Fig. 5 Si2p XPS spectra of the nc-Si:H thin films prepared at the H_2 flow rates of **a** 45, **b** 60, **c** 75, and **d** 90 sccm

The increase in the H_2 flow rate up to 90 sccm at a fixed SiH_4 flow rate contributed to the generation of larger Si crystallites. On the other hand, at the H_2 flow rate of 45 sccm, Si crystallization did not proceed as well as it did at the H_2 flow rates of 60–90 sccm. This can be attributed to the relatively small proportion of H_2 gas in the plasma chamber. At the H_2 flow rate of 45 sccm, a larger amount of H^* radicals was required to form (or grow) Si crystallites in the films than those required at the higher flow rates. A certain quantity of hydrogen radicals is required to initiate (or continue) the crystallization at the surface of a-Si or Si nanocrystallites. The hydrogen at the surface of nanocrystallites etches out to produce desorbing H_2 gas molecules by the reaction with hydrogen radicals or SiH, SiH_2, and SiH_3, resulting in the production of dangling bonds at the surface, which is suitable for the attachment of Si-containing precursor radicals. However, a large number of Si–H_2 bonds and very few crystallites were observed in the films prepared at the H_2 flow rate of 45 sccm. This suggests that the molecules or radicals of the source gas produced 'string-like' Si-chains consisting of Si–H_2 bonds rather than 3-D Si nanocrystallites, as shown in Fig. 4b. The deficiency of hydrogen radicals is likely to be the reason for the polymeric features of the film.

However, at the H_2 flux of 90 sccm, the dominant polymeric features of the film showed that the amount of hydrogen radicals was insufficient to provide suitable atomic sites for the nucleation/growth of Si crystallites, and hence the volume fraction of crystallites was almost zero.

3.3 Optical Features

Figure 6 shows the PL spectra of the nc-Si:H thin films. Prominent PL peaks were observed for the films prepared at the H_2 flow rates of (a) 45, (b) 60, (c) 75, and (d) 100 sccm, and the peak position shifted gradually from ~ 620 to ~ 690 nm with an increase in the H_2 flow rate from 60 to 90 sccm. However, the film prepared at the H_2 flow rate of 45 sccm did not show any noticeable PL phenomena, which can be attributed to the low concentration of Si nanocrystallites in it. As mentioned earlier, no Si nanocrystallites were observed in this film.

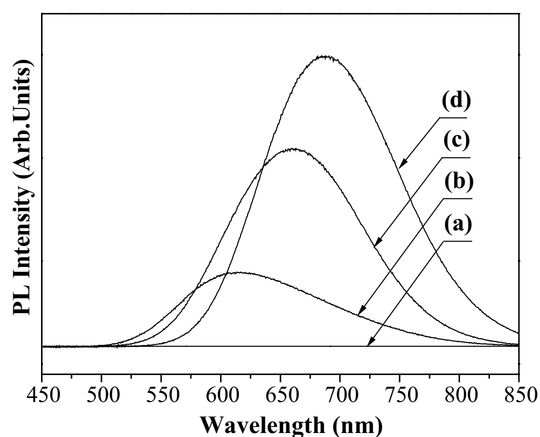

Fig. 6 PL spectra of the nc-Si films prepared at the H_2 flow rates of **a** 45, **b** 60, **c** 75, and **d** 90 sccm

The films prepared at the H_2 flow rates of 60, 75, and 90 sccm showed intense PL peaks at ~ 617, 662, and ~ 687 nm, respectively. However, the film prepared at the H_2 flow rate of 45 sccm did not show any noticeable PL phenomena because of its low Si nanocrystallite concentration. The shift in the PL peaks with an increase in the H_2 flow rate correlated well with the change in the size of the Si nanocrystallites with the H_2 flow rate. The Si crystallite size increased from 2.3 to 3.3 nm with an increase in the H_2 flow rate from 60 to 90 sccm.

According to the effective mass theory, the energy bandgap (E) for the crystallite size of nc-Si can be expressed as $E(\mathrm{eV}) = 1.56 + 2.40/d^2$ [19], where 1.56 represents the bandgap of bulk amorphous Si, d is the crystallite size, and 2.40 is the confinement parameter. The sizes of the Si nanocrystallites of the films prepared with the H_2 flow rates of 60, 75, and 90 sccm were 2.3, 2.8, and 3.2 nm, respectively, and the corresponding nc-Si bandgaps were 2.00, 1.87, and 1.80 eV, respectively. Hence, the position of the PL peaks matched well with the nc-Si:H size of the films.

The QCE increases the bandgap of nanocrystallites, increasing the oscillator strength, and hence giving rise to efficient and visible luminescence [20]. The crystallite size distribution is believed to be responsible for the broad PL spectra of nc-Si: H films, which typically exhibit an FWHM of 300–400 meV [6]. Various efforts have been made to explain the effect of size distribution on the PL spectrum of c-Si: H films [21]. The PL spectra of the c-Si: H films were analyzed to estimate the average size of the nanocrystallites [19]. The results so obtained were consistent with the Raman spectroscopy and TEM results.

3.4 Electrical Features

Figure 7 shows the bias ln(I)–V curves of the Al:ZnO/nc-Si:H/p-type Si wafer/Al contacts fabricated from the films prepared at the H_2 flow rates of (a) 45, (b) 60, (c) 75, and (d) 90 sccm. With an increase in the forward bias, the current increased and the excitation of the electrons in the nc-Si: H layer as well as the resultant recombination of radiation increased significantly. The nc-Si:H films with higher H_2 flow rates showed higher current density in the forward bias region. These results indicate that these nc-Si:H films had a sufficient number of crystallites large enough for the excitation under these experimental conditions.

The linear region of the ln I–V plot of device is a good indicator of the presence of rectifier junction behavior, and

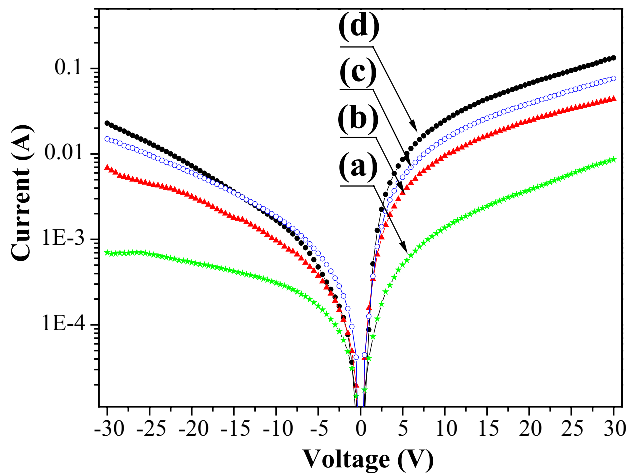

Fig. 7 The current versus voltage characteristics of the Al:ZnO/nc-Si:H/p-type Si wafer/Al contacts. The films were prepared at the H_2 flow rates of **a** 45, **b** 60, **c** 75, and **d** 90 sccm

a linearity deviation at high voltages represents the series resistance effect [22]. With an increase in the H_2 flow rate, the Ohmic behavior of the device became more prominent and the high injection region shifted towards lower voltages. In addition, an increase in the H_2 flow rate resulted in a steady increase in the current of the nc-Si:H films. The films with Si nanocrystallites showed ~ 10 times higher current than the a-Si films. This indicates that the nc-Si:H films deposited at higher H_2 flow rates were structurally modified. This drastic increase in the current gain of the films deposited at higher H_2 flow rates can be attributed to the increase in their crystalline fraction and size.

4 Conclusion

The size of the Si nanocrystallites of the nc-Si:H films prepared in this study increased with an increase in the H_2 flow rate from 45 to 90 sccm. The crystallite size of nc-Si:H films depends on their relative Si–H bond fraction, $[Si-H]/\sum[Si-H_n]_{n=1,2,3}$, which is affected by the H_2 flow rate. With an increase in the H_2 flow rate from 60 to 90 sccm, the size of the Si nanocrystallites increased from ~ 2.3 to ~ 3.3 nm, while the PL emission wavelength varied from ~ 617 to ~ 687 nm. The wavelength of nc-Si:H films is related to the average size of their nanocrystallites. The current of the nc-Si:H films increased with forward bias depending on their crystallite size and volume fraction. At the H_2 flow rate of 45 sccm, the formation of nanocrystalline Si was prevented, and the film became amorphous. This suggests that a certain amount of hydrogen radicals is essential for both the nucleation and growth of Si nanocrystallites in a-Si:H films.

References

1. G. Cicala, P. Capezzuto, G. Bruno, Thin Solid Films **337**, 59 (1999)
2. Y. Chen, S. Wagner, Appl. Phys. Lett. **75**, 1125 (1999)
3. Y. Yuan, W. Zhao, J. Ma, Z. Yang, W. Li, K. Zhang, Surf. Coat. Technol. **320**, 362 (2017)
4. S.W. Park, E.C. Cho, D.Y. Song, G. Conibeer, M.A. Green, Sol. Energy. Mater. Sol. Cell **93**, 684 (2009)
5. A. Shah, P. Torres, R. Tscharner, N. Wyrsch, H. Keppner, Science **285**, 692 (1999)
6. Y. Yu, G. Fan, A. Fermi, R. Mazzaro, V. Morandi, P. Ceroni, D.-M. Smilgies, B.A. Korgel, J. Phys. Chem. C **121**, 23240 (2017)
7. B. von Roedern, L. Ley, M. Cardona, Phys. Rev. Lett. **39**, 1576 (1977)
8. U.K. Das, P. Chaudhuri, Chem. Phys. Lett. **298**, 211 (1998)
9. S. Oda, Adv. Colloid Interface. **71**, 31 (1997)
10. W. Weia, G. Xub, J. Wang, T. Wang, Vacuum **81**, 656 (2007)
11. S. Veprek, F.A. Sarott, Z. Iqbal, Phys. Rev. B **36**, 3344 (1987)
12. Y. He, C. Yin, G. Cheng, L. Wang, X. Liu, G.Y. Hu, J. Appl. Phys. **75**, 797 (1994)
13. S. Veprek, Z. Iqbal, F.A. Sarott, Philos. Mag. B **45**, 137 (1982)
14. X.L. Wu, G.G. Siu, S. Tong, X.N. Liu, F. Yan, S.S. Jiang, D. Feng, Appl. Phys. Lett. **69**, 523 (1996)
15. D. Beeman, R. Tsu, M.F. Tporpe, Phys. Rev. B **32**, 874 (1985)
16. M.H. Brodsky, M. Cardona, J.J. Cuomo, Phys. Rev. B **16**, 3556 (1977)
17. F. Rochet, G. Dufour, H. Roulet, B. Pelloie, J. Perriere, E. Fogarassy, A. Slaoui, M. Froment, Phys. Rev. B **37**, 6468 (1988)
18. J.-H. Shim, S.-I. Im, N.-H. Cho, Appl. Sur. Sci. **234**, 268 (2004)
19. H.-S. Kwack, Y. Sun, Y.-H. Cho, N.-M. Park, S.-J. Park, Appl. Phys. Lett. **83**, 2901 (2003)
20. P. Mishra, K.P. Jain, Mater. Sci. Eng., B **95**, 202 (2002)
21. A.G. Cullis, L.T. Canham, Nature **353**, 335 (1991)
22. A.S. Kavasoglu, N. Kavasoglu, A.O. Kodolbas, O. Birgi, O. Oktu, S. Oktik, Microelectron. Eng. **87**(2), 108 (2010)

Publisher's Note Springer Nature remains neutral with regard to jurisdictional claims in published maps and institutional affiliations.